An Efficient, Steady, Subsonic Collocation Method for Solving Lifting-Surface Problems

ATLEE M. CUNNINGHAM JR.*
General Dynamics Corporation, Fort Worth, Texas

In the collocation approach for solving the integral equation of steady subsonic lifting-surface theory, accurate integration of the product of the kernel and pressure functions over the wing surface is required before a stable solution can be achieved. A Gaussian quadrature integration technique is developed which includes correction terms that account for the error incurred while integrating through the singularity and discontinuity of the kernel function. It is shown how inconsistent treatment of the chordwise discontinuity will cause the spanwise integration to diverge with an increasing number of integration chords. An optimum relationship is given between the number of chordwise downwash points and a larger number of chordwise integration points. Also given is an empirically determined optimum ratio of spanwise to chordwise control points based on planform geometry. By comparison with experiment and other theories, the method is shown to be both stable and accurate as well as more efficient than methods based on finite aerodynamic element representations of lifting surfaces.

Nomenclature

a_{nm}	= assumed pressure series coefficients
$(A_{nm})_{ir}$	= influence matrix element
b_0	= root semichord
$b(\eta)$	= semichord at span station
J	= integration points/integration chord ξ_j
$K(x-\xi, y-\eta, M)$	= subsonic steady kernel function
M	= freestream Mach number
$\bar{m}$	= downwash points/chord $\mathbf{x}_i$
$\bar{n}$	= total downwash chords $\mathbf{y}_r$
NC	= $\bar{m}$
NS	= downwash chords/semispan
R	= $[(\bar{x}-\bar{\xi})^2+\beta^2(\bar{y}-\bar{\eta})^2]^{1/2}$
s_0	= semispan
S	= total integration chords η_s
U_∞	= freestream velocity
$\Delta p(\xi,\eta)$	= pressure difference at point ξ,η
$w(x,y)$	= downwash at point x,y
$\bar{W}(x,y)$	= $4\pi\rho U_\infty w(x,y)$
X_{cp}	= chordwise location of the aerodynamic center as a fraction of the root chord
Y_{cp}	= spanwise location of the aerodynamic center as a fraction of the semispan
x,y	= downwash point location
ξ,η	= integration point location
$\bar{x},\bar{y}$	= (x/b_0), (y/b_0)
$\bar{\xi},\bar{\eta}$	= (ξ/b_0), (η/b_0)
$\mathbf{x},\mathbf{y}$	= $[x-x_m(y)]/b(y)$, (y/s_0)
$\boldsymbol{\xi},\boldsymbol{\eta}$	= $[\xi-\xi_m(\eta)]/b(\eta)$, (η/s_0)
$x_m(y),\xi_m(\eta)$	= mean chord location at span stations y and η, respectively
ρ	= freestream density
β	= $(1-M^2)^{1/2}$

Introduction

THE principal equation in subsonic lifting-surface theory is the integral equation that relates the pressure-difference distribution over the surface of interest with the normal velocity or downwash induced by the surface. This equation may be expressed as

$$w(x,y)=\frac{1}{4\rho U_\infty}\iint_{S_W}\Delta p(\xi,\eta)K(x-\xi,y-\eta,M)d\xi d\eta \quad (1)$$

where the pressure difference (or lift) $\Delta p(\xi,\eta)$ is unknown. The downwash $w(x,y)$ in steady linearized theory is equal to the freestream velocity U_∞ multiplied by the local streamwise slope of the surface at point x,y. The kernel function $K(x-\xi,y-\eta,M)$ is a function of Mach number and position relative to the downwash point x,y.

In determining subsonic aerodynamic load distributions over lifting surfaces, one may solve Eq. (1) by the use of either finite aerodynamic elements[1,2] or an assumed solution (or collocation method) with unknown coefficients.[3-9] Of the two approaches, the collocation method is the most difficult to apply, but it does provide a more efficient and economical means by which a solution can be obtained, as discussed by Stark.[9]

In the collocation approach for solving Eq. (1), which is the subject of this paper, one of the most critical steps is the integration of the product of the kernel and pressure functions. A wide variety of methods exist for performing the integration, as was pointed out in the survey paper by Landahl and Stark.[10] In most cases, the integral is evaluated as a summation of point values of the integrand; hence, the methods which are the most efficient are those that require the smallest number of integration points for a fixed number of downwash or collocation points. Because of the large amount of computer time consumed in evaluating the oscillatory kernel function, this aspect becomes more important for unsteady flow, particularly if one is concerned with aeroelastic optimization.

One of the best known collocation methods is that developed by Watkins, Woolston, and H. J. Cunningham.[8] In this method, a large number of integration points (over 200 on the total wing), independent of the number of downwash points, are used. The number of integration points required by the method of Hsu,[5] nominally less than 100, is only slightly greater than twice the number of downwash points on the semispan. Comparison of these two methods at the Fort Worth Division of General Dynamics has verified that the Watkins et al. method is significantly more time-consuming than the latter method on comparable problems. Thus,

Presented as Paper 70-191 at the AIAA 8th Aerospace Sciences Meeting, New York, January 19–21, 1970; submitted February 19, 1970; revision received July 20, 1970.

* Senior Structures Engineer, Fort Worth Division. Member AIAA.

for problems incurred in aeroelastic work, where the camber induced through static bending or natural modes is of low-order curvature, Hsu's method provides a particularly efficient means of predicting steady or oscillatory pressure distributions. For problems where highly cambered surfaces are encountered, which require approximately ten or more chordwise pressure functions, the advantages would not be as great. (For further discussion of this aspect, see Refs. 17 and 18).

Although the method of Hsu is efficient and applicable to both steady and oscillatory flow, it does contain instabilities, as is discussed by Rowe.[6] In order to stabilize Hsu's method without resorting to an increased number of integration points as Rowe has done, the integration technique has been reassessed. As a result, a new equation has been derived for the quadrature integration of Eq. (1), with the appropriate pressure functions for both steady and oscillatory flow as given by A. M. Cunningham.[7]

In this paper, a summary of the new integration scheme of Ref. 7 is presented for steady flow. The method yields correction terms, added to the basic quadrature integration, that account for the error incurred while integrating through the singularity and discontinuity of the kernel function. The optimum sets of excess chordwise integration points (greater than the number of chordwise control points) are discussed and an explanation is given for the erratic variation, as discussed by Rowe, of the chordwise integral with increasing number of integration points. Finally, through comparisons with experimental data, an empirical rule is determined which specifies that the optimum ratio of spanwise-to-chordwise control points is a simple and predictable function of planform geometry and Mach number. By comparison with two finite element methods,[1,2] the present method is shown to be the most efficient of the three.

Integral Equation

The appropriate integral equation for steady subsonic potential flow may be written as

$$\bar{W}(\bar{x},\bar{y}) = \int_{-1}^{1} \frac{b_0}{s_0} \frac{\partial}{\partial \mathbf{n}} \left\{ \int_{-1}^{1} \Delta p(\xi,\mathbf{n}) \left[1 + \frac{\bar{x} - \xi}{R} \right] \times \frac{b(\mathbf{n})}{b_0} \, d\xi \right\} \frac{d\mathbf{n}}{(y - \mathbf{n})} \quad (2)$$

Following the practice of Hsu and others, the pressure distribution over the planform is assumed as

$$\Delta p(\xi,\mathbf{n}) = \frac{4\rho U_\infty^2}{b(\mathbf{n})} s_0 (1 - \mathbf{n}^2)^{1/2} \left[g_0(\mathbf{n}) \left(\frac{1 - \xi}{1 + \xi} \right)^{1/2} + g_1(\mathbf{n})(1 - \xi^2)^{1/2} + g_2(\mathbf{n})\xi(1 - \xi^2)^{1/2} + \ldots \right] \quad (3a)$$

where

$$g_n(\mathbf{n}) = [a_{n0} + a_{n1}\mathbf{n} + a_{n2}\mathbf{n}^2 + \ldots] \quad (3b)$$

(For further discussion on spanwise functions, see Ref. 18 in this volume.) Inserting Eq. (3) into (2) yields the working form of the steady-state integral equation for planar surfaces:

$$\bar{W}(\bar{x},\bar{y}) = 4\rho U_\infty^2 \int_{-1}^{1} \frac{\partial}{\partial \mathbf{n}} \left\{ (1 - \mathbf{n}^2)^{1/2} \int_{-1}^{1} \left[g_0(\mathbf{n}) \left(\frac{1 - \xi}{1 + \xi} \right)^{1/2} + g_1(\mathbf{n})(1 - \xi^2)^{1/2} + \ldots \right] \left[1 + \frac{\bar{x} - \xi}{R} \right] d\xi \right\} \frac{d\mathbf{n}}{\mathbf{y} - \mathbf{n}} \quad (4)$$

where $\xi,\mathbf{n}$ are coordinates in the transformed plane (see Fig. 1). If a symmetric loading is considered, only the even powers of $\mathbf{n}$ in the $g_n(\mathbf{n})$ functions are retained. For antisymmetric loading, the odd powers of $\mathbf{n}$ are used. This reduces the unknown coefficients by a factor of two as is common practice.

In Eq. (4), the terms $(1 - \xi)^{1/2}/(1 + \xi)^{1/2}$ and $(1 - \mathbf{n}^2)^{1/2}$ constitute weighting functions that allow the use of Gauss-Mehler quadrature integration formulas. Such an approach was taken by Hsu[5] to develop a surprisingly simple method for evaluating Eq. (4) and the more complex unsteady form of the equation. His treatment of the spanwise integral will be used in the following integration of Eq. (4); however, the chordwise evaluation will be entirely new.

Integration of the Equation

If the chordwise integral in Eq. (4) is denoted as $G(\mathbf{y},\mathbf{n})$ the spanwise integral formula of Hsu[5] is

$$\fint_{-1}^{1} \frac{\partial}{\partial \mathbf{n}} \left[(1 - \mathbf{n}^2)^{1/2} G(\mathbf{y},\mathbf{n}) \right] \frac{d\mathbf{n}}{\mathbf{y} - \mathbf{n}} = -\frac{\pi}{S} \sum_{s=1}^{S}{}' \times \frac{(1 - \mathbf{n}_s^2) G(\mathbf{y}_r,\mathbf{n}_s)}{(\mathbf{y}_r - \mathbf{n}_s)^2} + \pi S G(\mathbf{y}_r,\mathbf{y}_r) \quad (5)$$

where $\fint$ refers to integrals of the Cauchy type and

$\mathbf{y}_r = -\cos r\pi/S,\ r = 1, 2, \ldots, (S - 1)$

$\mathbf{n}_s = -\cos[(2s - 1)/2S]\pi,\ s = 1, 2, \ldots, S$

S = total number of integration stations

$\mathbf{y}_r$ = downwash span station

$\mathbf{n}_s$ = integration span station

The restriction of $G(\mathbf{y}_r,\mathbf{n}_s)$ is that it be a polynomial of degree $(2S - 1)$ or less for evaluation of the integral to be exact. As the degree of $G(\mathbf{y}_r,\mathbf{n}_s)$ increases above (2S-1), the error increases accordingly. If the evaluation of the chordwise integral is properly performed then the results of Eq. (5) should not be in doubt.

Treatment of the Chordwise Discontinuity

From Eq. (4), the G function is

$$G(\mathbf{y},\mathbf{n}) = \int_{-1}^{1} \left[g_0(\mathbf{n}) \left(\frac{1 - \xi}{1 + \xi} \right)^{1/2} + g_1(\mathbf{n})(1 - \xi^2)^{1/2} + \ldots \right] \times \left[1 + \frac{\bar{x} - \xi}{R} \right] d\xi \quad (6)$$

An examination of Eq. (6) reveals that a discontinuity exists along $\bar{\eta} = \bar{y}$ at $\xi = \bar{x}$. Provided this discontinuity can be removed or sufficiently "softened," the integral may be evaluated with a Gauss-Mehler quadrature formula[11] used by Hsu:

$$\int_{-1}^{1} \left(\frac{1 - \xi}{1 + \xi} \right)^{1/2} f(\xi) d\xi = \frac{2\pi}{2J + 1} \sum_{j=1}^{J} (1 - \xi_j) f(\xi_j) \quad (7)$$

where

$$\xi_j = -\cos[\pi(2j - 1)/(2J + 1)],\ j = 1, 2, \ldots, J$$

Denoting $\phi(\xi,\mathbf{n})$ as the polynomial of the integrand of Eq. (6)

$$\phi(\xi,\mathbf{n}) = \left(\frac{1 - \xi}{1 + \xi} \right)^{1/2} [g_0(\mathbf{n}) + g_1(\mathbf{n})(1 + \xi) + \ldots] \quad (8)$$

the discontinuity can be properly eliminated in the following manner:

$$G(\mathbf{y},\mathbf{n}) = \int_{-1}^{1} [\phi(\xi,\mathbf{n}) - \phi(\xi,\mathbf{y})] \left[1 + \frac{\bar{x} - \xi}{R} \right] d\xi + \int_{-1}^{1} \phi(\xi,y) \left[1 + \frac{\bar{x} - \xi}{R} \right] d\xi \quad (9)$$

However, the resulting integral of $\phi(\xi,\mathbf{y})$ that must be inte-

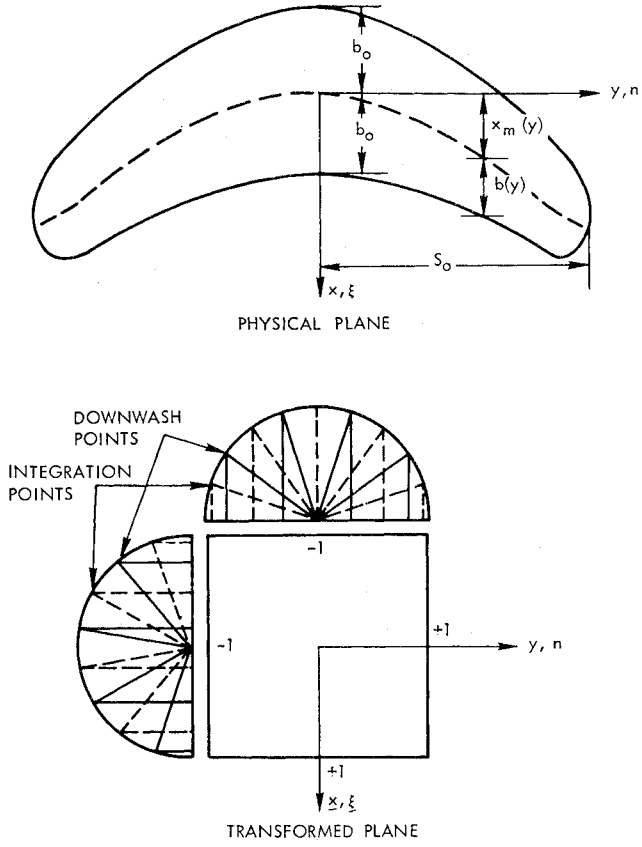

Fig. 1 Arbitrary planform in physical and transformed plane.

grated analytically still contains the discontinuity and is no simpler to evaluate than Eq. (6). Let us instead, consider the Taylor series expansion of $\phi(\xi,\mathbf{y})$ about $\xi = \mathbf{x}$. Equation (9) then becomes

$$G(\mathbf{y},\mathbf{n}) = \int_{-1}^{1} \left\{ \phi(\xi,\mathbf{n}) - \left[\phi(\mathbf{x},\mathbf{y}) + \frac{b_0(\bar{\xi}-\bar{x})}{b(\mathbf{n})}\phi_x(\mathbf{x},\mathbf{y}) + \frac{b_0^2(\bar{\xi}-\bar{x})^2}{2![b(\mathbf{n})]^2}\phi_{xx}(\mathbf{x},\mathbf{y}) + \ldots \right] \right\} \frac{\bar{x}-\bar{\xi}}{R}\,d\xi + \int_{-1}^{1} \phi(\xi,\mathbf{n})d\xi + \int_{-1}^{1} \left[\phi(\mathbf{x},\mathbf{y}) + \frac{b_0(\bar{\xi}-\bar{x})}{b(\mathbf{n})}\phi_x(\mathbf{x},\mathbf{y}) + \frac{b_0^2(\bar{\xi}-\bar{x})^2}{2![b(\mathbf{n})]^2}\phi_{xx}(\mathbf{x},\mathbf{y}) + \ldots \right] \frac{\bar{x}-\bar{\xi}}{R}\,d\xi \quad (10)$$

Since $\phi(\xi,\mathbf{y})$ is analytic in ξ, an infinite or at least a converged Taylor series expansion is required in Eq. (10). However, only a finite series will be considered in the following discussion, while keeping in mind that higher-order terms may be treated in the same manner.

In Eq. (10), the first and second integrals may now be evaluated with a Gauss-Mehler quadrature formula. The third set is simple enough so that analytic integration can be performed.

If only the first two terms of the Taylor series expansion of $\phi(\xi,\mathbf{y})$ are considered, the resulting integrand will be smooth and continuous throughout the interval $(-1 \leq \xi \leq +1)$ but will contain singular second- and higher-order derivatives at the downwash point along $\mathbf{n} = \mathbf{y}$. If $G(\mathbf{y},\mathbf{y})$ and $G(\mathbf{y},\mathbf{n})$ are evaluated consistently, the error produced in evaluating Eq. (4) with the formula given in Eq. (5) should be minimized. If the same technique is not used, then the equation

$$[G(\mathbf{y},\mathbf{n}) - G(\mathbf{y},\mathbf{y})]/(\mathbf{y}-\mathbf{n}) = -G'(\mathbf{y},\mathbf{y}) - (\mathbf{n}-\mathbf{y})/2!G''(\mathbf{y},\mathbf{y}) - \ldots$$

for which

$$\lim_{\eta\to\mathbf{y}} \left\{ \frac{G(\mathbf{y},\mathbf{n}) - G(\mathbf{y},\mathbf{y})}{\mathbf{y}-\mathbf{n}} \right\} = -G'(\mathbf{y},\mathbf{y}) \quad (11)$$

on which Hsu[5] bases the proof of convergence of Eq. (5), is on longer valid but is singular at $\mathbf{n} = \mathbf{y}$. What actually happens is that the Gaussian quadrature integration of $G(\mathbf{y},\mathbf{n})$ is in error by an amount $E(\mathbf{n})$. Hence the limit yields

$$\lim_{\eta\to\mathbf{y}} \{G(\mathbf{y},\mathbf{n})\}_n = \{G(\mathbf{y},\mathbf{y})\}_n = \{G(\mathbf{y},\mathbf{y})\}_e + E(\mathbf{y}) \quad (12)$$

where the subscripts n and e denote numerical (quadrature integration) and exact integrals. Since the $G(\mathbf{y},\mathbf{y})$ function as evaluated by both Hsu and Rowe is much more exact than $G(\mathbf{y},\mathbf{n})$ (except for Rowe's converged integral), the following limit occurs:

$$\lim_{\eta\to\mathbf{y}} \left\{ \frac{G(\mathbf{y},\mathbf{n})_n - G(\mathbf{y},\mathbf{y})_e}{\mathbf{y}-\mathbf{n}} \right\} = E(\mathbf{y}) \lim_{\eta\to\mathbf{y}} \left\{ \frac{1}{\mathbf{y}-\mathbf{n}} \right\} = \infty \quad (13)$$

Thus, Eq. (5) will diverge as the number of $\mathbf{n}_s$ stations are increased if $G(\mathbf{y},\mathbf{n})$ has not sufficiently converged such that Eq. (11) is satisfied. As the number of chordwise integration points are increased such that the error term is sufficiently small in Eq. (12), then increasing the number of integration chords would show solution convergence. This could be carried out only so far until the two integration chords next to the downwash chord are close enough to cause the error to begin to diverge again, since $E(\mathbf{y})$ would still be finite.

In Rowe's work[2] on removing the instability in Hsu's theory, he shows that for a wing with an aspect ratio of unity in steady subsonic flow for four integration points/chord ξ_i, four downwash points/chord $\mathbf{x}_i$, and the solution diverges as the downwash chords $\mathbf{y}_r$, are increased from 4 to 8.† In this problem, the integration chords $\mathbf{n}_s$ are increased from 9 to 17. For the same wing he also shows that if the integration points per chord are increased to 13 such that the chordwise integral has sufficiently converged, the solution converges for eight downwash chords. In his first attempt, the error term was large since only four integration points were used to evaluate $G(\mathbf{y},\mathbf{n})$. Thus, as chords were chosen closer together, the smallest value of $(\mathbf{y}-\mathbf{n})$ decreased, causing an increase of the error incurred in the spanwise integral (see Eq. 13). The error was further increased because $E(\mathbf{n})$ became larger as $\mathbf{n} \to \mathbf{y}$. In the second attempt, the error term was sufficiently small to allow convergence of the spanwise integral, as would be expected since the downwash chords, and hence the integration chords, were increased.

Because of the nature of the error term associated with the Gauss-Mehler integral formula and the confirming results of Rowe, it is felt that the most efficient manner in which to evaluate $G(\mathbf{y},\mathbf{y})$ and $G(\mathbf{y},\mathbf{n})$ is to use exactly the same approach for each, such that

$$\lim_{\eta\to\mathbf{y}} \{G(\mathbf{y},\mathbf{n})\} = G(\mathbf{y},\mathbf{y}) \quad (14)$$

is a true statement. This is equivalent to stating that the error terms $E(\mathbf{n})$ and $E(\mathbf{y})$ for $G(\mathbf{y},\mathbf{n})$ and $G(\mathbf{y},\mathbf{y})$, respectively, must satisfy the condition.

$$\lim_{\eta\to\mathbf{y}} \{E(\mathbf{n})\} = E(\mathbf{y}) \quad (15)$$

Such a philosophy will be followed in the next subsection.

Chordwise Integral

The chordwise integration will be first evaluated to obtain $G(\mathbf{y},\mathbf{n})$; then $\mathbf{n}$ will be set equal to $\mathbf{y}$ to obtain $G(\mathbf{y},\mathbf{y})$. In this

† Downwash chords/semispan.

manner, it is assured that Eqs. (14) and (15) will be satisfied. However, it must be clear that although these equations are satisfied, as $\mathbf{n} \to \mathbf{y}$, the error terms are converging but are not necessarily equal for $\mathbf{y} \neq \mathbf{n}$; thus, accurate evaluation of $G(\mathbf{y},\mathbf{n})$ and $G(\mathbf{y},\mathbf{y})$ is still required for accurate results.

To begin, Eq. (10) is rewritten in a more tractable form: where the analytic integrals $H_0(\bar{x},\bar{\eta})$ and $H_1(\bar{x},\bar{\eta})$ are

$$H_0(\bar{x},\bar{\eta}) = \int_{-1}^{1} \frac{\bar{x} - \bar{\xi}}{[(\bar{x} - \bar{\xi})^2 + \beta^2(\bar{y} - \bar{\eta})]^{2\,1/2}}\, d\bar{\xi}$$

or

$$G(\mathbf{y},\mathbf{n}) = \int_{-1}^{1} \left\{ \phi(\xi,\mathbf{n}) - \left[\phi(\mathbf{x},\mathbf{y}) + \frac{b_0(\bar{x} - \bar{\xi})}{b(\mathbf{n})}\, \phi_x(\mathbf{x},\mathbf{y}) + \ldots \right] \right\} \frac{\bar{x} - \bar{\xi}}{R}\, d\bar{\xi} + \int_{-1}^{1} \phi(\xi,\mathbf{n}) d\bar{\xi} + [\phi(\mathbf{x},\mathbf{y}) H_0(\bar{x},\bar{\eta}) + \phi_x(\bar{x},\mathbf{y}) H_1(\bar{x},\bar{\eta}) + \ldots] \quad (16)$$

$$H_0(\bar{x},\bar{\eta}) = \frac{b_0}{b(\mathbf{n})} \{ [(\bar{x} - \bar{\xi}_1)^2 + \beta^2(\bar{y} - \bar{\eta})^2]^{1/2} - [(\bar{\xi}_t - \bar{x})^2 + \beta^2(\bar{y} - \bar{\eta})^2]^{1/2} \} \quad (17a)$$

and

$$H_1(\bar{x},\bar{\eta}) = \frac{b_0}{b(\mathbf{n})} \int_{-1}^{1} \frac{-(\bar{x} - \bar{\xi})^2}{[(\bar{x} - \bar{\xi})^2 + \beta^2(\bar{y} - \bar{\eta})^2]^{1/2}}\, d\bar{\xi}$$

or

$$H_1(\bar{x},\bar{\eta}) = -\left[\frac{b_0}{b(\mathbf{n})}\right]^2 \left\{ \frac{\bar{x} - \bar{\xi}_1}{2} [(\bar{x} - \bar{\xi}_1)^2 + \beta^2(\bar{y} - \bar{\eta})^2]^{1/2} + \frac{\bar{\xi}_t - \bar{x}}{2} [(\bar{\xi}_t - \bar{x})^2 + \beta^2(\bar{y} - \bar{\eta})^2]^{1/2} - \frac{\beta^2(\bar{y} - \bar{\eta})^2}{2} \times \left[\ln \left| \frac{[(\bar{x} - \bar{\xi}_1)^2 + \beta^2(\bar{y} - \bar{\eta})^2]^{1/2} + (\bar{x} - \bar{\xi}_1)}{[(\bar{\xi}_t - \bar{x})^2 + \beta^2(\bar{y} - \bar{\eta})^2]^{1/2} - (\bar{\xi}_t - \bar{x})} \right| \right] \right\} \quad (17b)$$

where $\bar{\xi}_1$ and $\bar{\xi}_t$ are the leading and trailing edge locations at $\mathbf{n}$ and

$$\phi(\mathbf{x},\mathbf{y}) = \left(\frac{1 - \mathbf{x}}{1 + \mathbf{x}}\right)^{1/2} [g_0(\mathbf{y}) + g_1(\mathbf{y})(1 + \mathbf{x}) + \ldots] \quad (17c)$$

$$\phi_x(\mathbf{x},\mathbf{y}) = \frac{\partial}{\partial \mathbf{x}} \{\phi(\mathbf{x},\mathbf{y})\} \quad (17d)$$

Higher-order functions H_2, H_3, etc. may be obtained in precisely the same manner as H_0 and H_1. The remaining integrals in Eq. (16) are evaluated by use of the quadrature formula [Eq. (7)] to give

$$G(\mathbf{y},\mathbf{n}) = \frac{2\pi}{2J+1} \sum_{j=1}^{J} [g_0(\mathbf{n})(1 - \xi_j) + g_1(\mathbf{n})(1 - \xi_j^2) + \ldots] \left[1 + \frac{\bar{x}_i - \bar{\xi}_j}{R_{ij}} \right] + \phi(\mathbf{x}_i,\mathbf{y}) \left\{ H_0(\bar{x}_i,\bar{\eta}) + \frac{2\pi}{2J+1} \sum_{j=1}^{J} \frac{(1 - \xi_j^2)^{1/2}(\bar{\xi}_j - \bar{x}_i)}{R_{ij}} \right\} + \phi_x(\mathbf{x}_i,\mathbf{y}) \left\{ H_1(\bar{x}_i,\bar{\eta}) + \frac{2\pi}{2J+1} \frac{b_0}{b(\mathbf{n})} \sum_{j=1}^{J} \frac{(1 - \xi_j^2)^{1/2}(\bar{\xi}_j - x_i)^2}{R_{ij}} \right\} + \ldots \quad (18a)$$

$$G(\mathbf{y},\mathbf{y}) = \frac{2\pi}{2J+1} \sum_{j=1}^{J} [g_0(\mathbf{y})(1 - \xi_j) + g_1(\mathbf{y})(1 - \xi_j^2) + \ldots] \left[1 + \frac{\mathbf{x}_i - \xi_j}{|\mathbf{x}_i - \xi_j|} \right] + \phi(\mathbf{x}_i,\mathbf{y}) \left\{ 2\mathbf{x}_i + \frac{2\pi}{2J+1} \sum_{j=1}^{J} \frac{(1 - \xi_j^2)^{1/2}(\xi_j - \mathbf{x}_i)}{|\mathbf{x}_i - \xi_j|} \right\} + \phi_x(\mathbf{x}_i,\mathbf{y}) \left\{ (1 + \mathbf{x}_i^2) - \frac{2\pi}{2J+1} \sum_{j=1}^{J} (1 - \xi_j^2)^{1/2} |\mathbf{x}_i - \xi_j| \right\} + \ldots \quad (18b)$$

The optimum downwash chord stations $\mathbf{x}_i$ are given by Hsu as

$$\mathbf{x}_i = -\cos\left(\pi \frac{2i}{2\bar{m}+1}\right), \quad i = 1, 2, \ldots, \bar{m} \quad (19)$$

thus completing the equations for the chordwise integrals, $G(\mathbf{y},\mathbf{n})$ and $G(\mathbf{y},\mathbf{y})$.

Equations (18a) and (18b) consist of two parts, of which the first is the direct application of the quadrature formula and the remainder is the set of correction terms. The correction terms may be expressed in series form as

$$\Psi_G(\mathbf{y},\mathbf{n}) = \sum_{p=0}^{P} \frac{1}{p!}\, \phi_{p(x)}(\mathbf{x}_i,\mathbf{y}) \left\{ H_p(\bar{x}_i,\bar{\eta}) + \frac{2\pi}{2J+1} \left[\frac{b_0}{b(\mathbf{n})}\right]^p \sum_{j=1}^{J} \frac{(1 - \xi_j^2)^{1/2}(\bar{\xi}_j - \bar{x}_i)^{p+1}}{R_{ij}} \right\} \quad (20a)$$

where $(P + 1)$ is the total number of terms used to approximate $\phi(\mathbf{n},\mathbf{y})$ in the neighborhood of $\xi = \mathbf{x}$. Likewise,

$$\Psi_G(\mathbf{y},\mathbf{y}) = \sum_{p=0}^{p} \frac{1}{p!}\, \phi_{p(x)}(\mathbf{x}_i,\mathbf{y}) \left\{ H_p(\bar{x}_i,\bar{y}) + \frac{2\pi}{2J+1} \sum_{j=1}^{J} \frac{(1 - \xi_j^2)^{1/2}(\xi_j - \mathbf{x}_i)^{p+1}}{|\mathbf{x}_i - \xi_j|} \right\} \quad (20b)$$

Inserting Eqs. (18) and (20) into (5) yields the final downwash expression:

$$\frac{\bar{W}(\bar{x}_i,\bar{y}_r)}{4\rho U_\infty{}^2} = -\frac{2\pi^2}{S(2J+1)}\sum_{s=1}^{S}\sum_{j=1}^{J}\frac{(1-\mathbf{n}_s{}^2)}{(\mathbf{y}_r-\mathbf{n}_s)^2}\left\{[g_0(\mathbf{n}_s)(1-\xi_j)+g_1(\mathbf{n}_s)(1-\xi_j{}^2)+\ldots]\times\right.$$
$$\left.\left[1+\frac{\bar{x}_i-\bar{\xi}_j}{[(\bar{x}_i-\bar{\xi}_j)^2+\beta^2(\bar{y}_r-\bar{\eta}_s)^2]^{1/2}}\right]\right\}+\frac{2\pi^2 S}{2J+1}\sum_{j=1}^{J}\left\{[g_0(\mathbf{y}_r)(1-\xi_j)+g_1(\mathbf{y}_r)(1-\xi_j{}^2)+\ldots]\left[1+\frac{\mathbf{x}_i-\xi_j}{|\mathbf{x}_i-\xi_j|}\right]\right\}-$$
$$\frac{\pi}{S}\sum_{s=1}^{S}\frac{(1-\mathbf{n}_s{}^2)}{(\mathbf{y}_r-\mathbf{n}_s)^2}\Psi_G(\mathbf{y}_r,\mathbf{n}_s)+S\pi\Psi_G(\mathbf{y}_r,\mathbf{y}_r) \quad (21)$$

In this form, the equation is not amendable to a convenient matrix form and must be broken up into a set of influence coefficients.

The equations resulting from the requirement for satisfying the tangential flow condition at the optimum control points on the semispan are arranged into the usual matrix equation,[5-7]

$$[(A_{nm})_{ir}]\{a_{nm}\} = -\pi\left\{\frac{\partial Z_{ir}}{\partial x}\right\}$$

and solved for the aerodynamic coefficients $\{a_{nm}\}$. This equation satisfies the linearized boundary conditions over the planar area of the wing of interest.

Excess Integration Points

In the last section, a final expression was given for the quadrature integration of the product of the pressure and kernel functions. In this expression, the integral was evaluated through a weighted $S \times J$ summation of point values of the integrand. It should be noted that in both the chordwise and spanwise integrations the downwash and integration points are interdigitated. The interdigital relationship is illustrated in Fig. 1, where the point locations are arrived at through an equiarc division of π radians.

If one wishes to increase the number of chordwise integration points per chord, care must be taken to ensure that the interdigital relationship is preserved. If this is not done, the J point summation will appear to locate the kernel function center at some point other than the downwash point. This effect is well illustrated in Rowe's study of the quadrature evaluation of a chordwise integral on a square wing near the tip.[6] In this case, the downwash chord is at $\mathbf{y}_8 = 0.9396$, the integration chord at $\mathbf{n}_9 = 0.9848$ and the downwash point at $\mathbf{x}_2 = 0.1736$. It is shown that for $J \leq 12$, the integral is wildly oscillating. For $J = 12$, one integral point, ξ_6, = -0.1874, is very close to the downwash point, and the next point, $\xi_7 = +0.06279$, is considerably aft; hence the integral evaluation for $G(\mathbf{y}_8,\mathbf{n}_9)$ would be expected to be low (as it is) because of the appearance of the kernel function center being aft of the true downwash point. At $J = 13$, the correct interdigitation is achieved for four downwash points/chord. The next value of J for which interdigitation would be achieved is 22, which unfortunately was not run. A third value of J, also not run, is 31, but the integral value for $J = 13$ and $J = 33$ are very nearly the same. Since for $J = 33$, the spacing is very close, small deviations in the interdigitation would not be significant. This is also illustrated at $J = 21$, which is very close to $J = 22$, the correct value. In this case, the integral value is also very close to the values at $J = 13$ and $J = 33$.

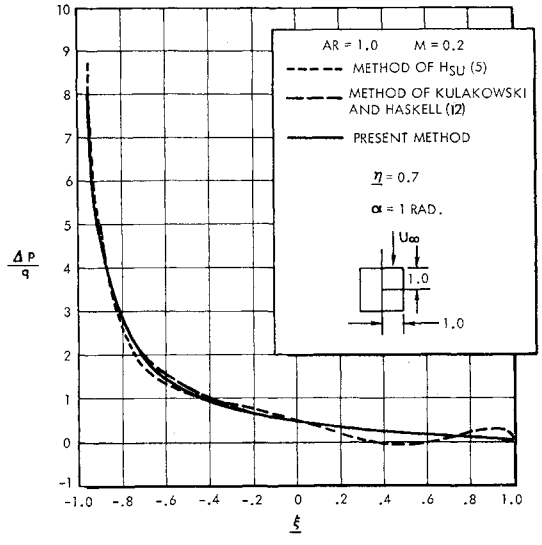

Fig. 2 Comparison of present theory with the methods of Hsu and Kulakowski and Haskell for a square wing with $NC = 5$ and $NS = 5$.

As a result of the above discussion it may be concluded that in choosing excess integration points, one should use only sets which preserve the interdigital nature of the downwash and integration points. The rule that ensures this relationship is expressed as

$$J = \text{integer value } [(\bar{m}+0.5)n] \quad (22)$$

where $n = 1, 3, 5, 7, \ldots$. [In Eq. (22), "integer value" refers to the truncated integer value of the expression inside the brackets.] Use of Eq. (22) in choosing excess integration points will avoid the oscillating integral values obtained by Rowe. Another way of viewing this equation is that it yields a larger set of integration points corresponding to a set of downwash points of which the $\bar{m}$ set is a subset.

Numerical Application of the Method

The first verification of the present method was through comparison with the original method of Hsu and with another subsonic collocation method. The second collocation method was that of Kulakowski and Haskell,[12] which is limited in planform application but has been shown repeatedly to give very good agreement with experiment. The results of this comparison for symmetric loading on a square wing at Mach 0.2 are shown in Fig. 2. In this comparison, the present method agrees very well with that of Kulakowski and Haskell and it does not show the oscillating tendency of Hsu's method. For all cases, the total downwash points/chord (NC) are 5 and the total downwash chords/semispan (NS) are 5. For the present method, only one correction term‡ ($P = 0$) and 5 integration points/chord were used ($J = 5$). On this basis, it appears that the chordwise integral can be evaluated with the standard integration points as given by Hsu with a more rigorous treatment of the discontinuity.

Next, the method was compared with experimental data on a rectangular wing of aspect ratio 3.[13] These results for symmetric loading are shown in Fig. 3, where very good agreement is found with 3 downwash points/chord ($NC = 3$) and 9 downwash chords/semispan ($NS = 9$). Again, only the first correction term and three integration points/chord were used. In this case, it was found that NS had to be larger than NC, as was shown by Rowe.

With the realization that aspect ratio seemed to be related to the ratio of NS to NC, the square-wing problem for sym-

‡ In this section, "correction term" refers only to those resulting from the chordwise integral.

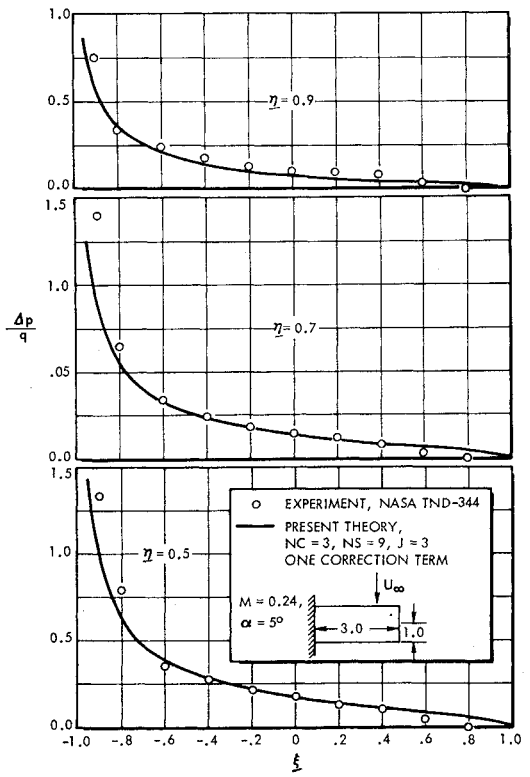

Fig. 3 Comparison of theoretical and experimental pressure distributions on a rectangular wing.

metric loading was again treated, but in this case the problem for Mach 0.8 as studied by Rowe[6] was considered. For $NC = 4$, the effect on C_L and X_{cp} of varying NS is shown in Fig. 4 along with the results of Rowe. It was found that by using one correction term the $J = 4$ and $J = 13$ cases converged on different values, thus illustrating the effect of not having the exact value of the chordwise integral $G(\mathbf{y},\mathbf{y})$. The impact of the more rigorous chordwise integration is well illustrated for this case since in Rowe's results both X_{cp} and C_L were extremely erratic for $NS = 4$ and $J = 4$. Note, however, that X_{cp} for $NS = 2$ and $J = 4$ is very close to the converged values of Rowe. For $J = 4$ or 13, the C_L values are very close, as is emphasized by the $\pm 0.25\%$ boundary. As a result, it is suspected that Mach number should affect the convergence characteristics as well as aspect ratio. Since increasing Mach number tends to shorten the y distances in the kernel function (βy), it was decided that the aspect ratio as seen by the kernel function (βAR) would likewise be affected. On this basis, $NS/NC = 0.5$ corresponded closely to $\beta(AR) = 0.6$. This result agrees with the trend shown by Lamar for the modified Multhopp theory.[4] Also, for the $AR = 3$ rectangular wing previously mentioned, $\beta(AR) = 2.92$, which is very close to the $NS/NC = 3$ that was used.

The method was then compared with experimental data on a swept-tapered wing.[14] Shown in Fig. 5 are the experimental and theoretical pressure distributions at $\mathbf{n} = 0.707$. In all cases, one correction term was used with $NC = 3$ and $J = 3$. For the first case, Mach 0.25, the most converged distribution is for $NS = 9$. For the second case, Mach 0.60, the most converged solution is for $NS = 9$, but this is not greatly different from that for $NS = 6$. For the third case, Mach = 0.80, $NS = 6$ yields the best results as indicated by the over-all pressure distributions. Since for these three cases, $\beta(AR)$ is 2.9, 2.4, and 1.8, respectively, and (NS/NC) is about 3, 2–3, and 2, respectively, the agreement shows that the $\beta(AR)$ rule still seems to hold.

In Fig. 6, a comparison is made between the present method, the doublet-lattice method of Albano and Rodden,[1] and ex-

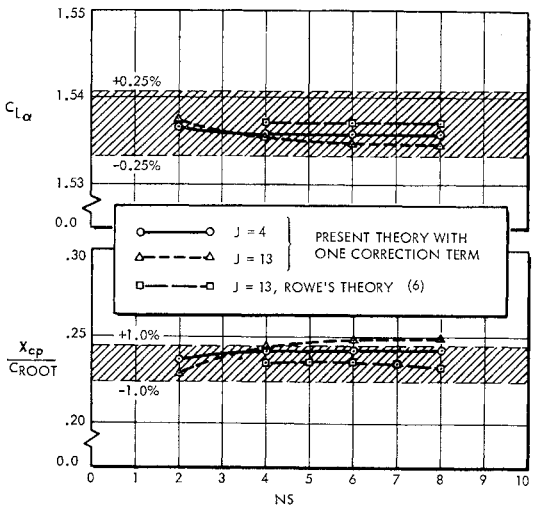

Fig. 4 Theoretical variation of C_L and X_{cp} with NS for $NC = 4$ on a square wing at $M = 0.80$.

periment.[14] The doublet-lattice solution was obtained with 48 panels distributed over the semispan. When compared with the array of only 18 downwash points required by the present method, one sees that equally valid results can be obtained with far fewer control points (and hence smaller matrices).

A more difficult case was then considered, that of an ogee wing for which experimental and other theoretical data was available.[15] The flow was essentially incompressible and the aspect ratio was 2.56. Hence, it was felt that a good solution should result if $NS/NC = 3$ was used. In Fig. 7, the computed and experimental results show that the solution was not sufficiently converged at $NS/NC = 3$ but was much better at $NS/NC = 5$. Since the distance R_0 is very influential in the kernel function it seems reasonable to assume that sweep should also influence solution convergence. The local

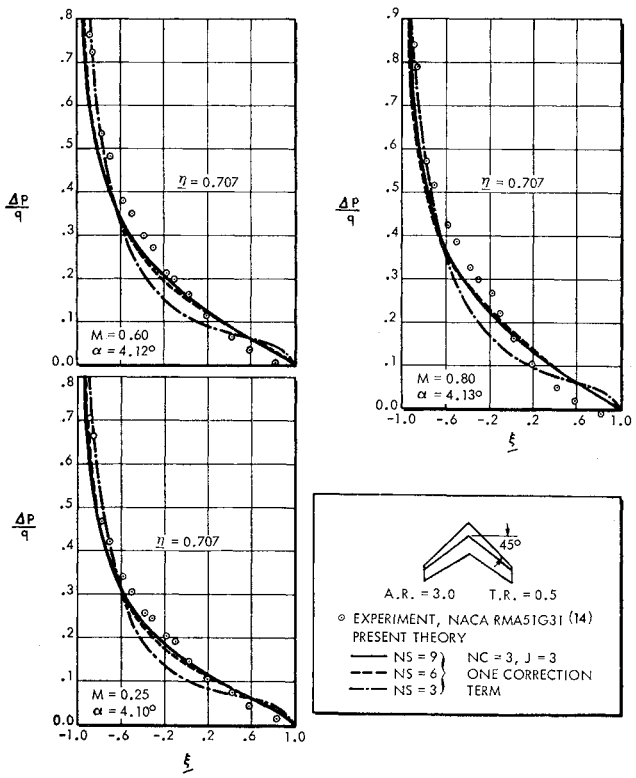

Fig. 5 Comparison of theoretical and experimental pressure distributions on a swept-tapered wing.

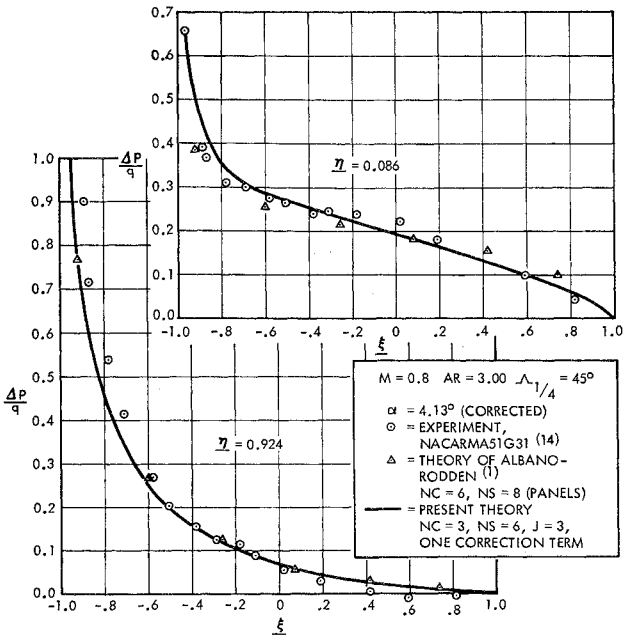

Fig. 6 Comparison of present theory with the doublet lattice method of Albano and Rodden and with experiment.

distance R'_0 is related to βy_0 as

$$R'_0 \approx |\beta y_0|/\cos[\Lambda(x_0,y_0)]$$

Hence, on the average, one would expect that the aspect ratio seen in the integral would appear to be of the form

$$(NC/NS)_{\text{conv}} \approx \beta(AR)/\cos|\Lambda_m| \qquad (23)$$

where Λ_m is the average of the absolute values of the leading and trailing edge sweep angles. Relating this with $(NS/NC)_{\text{conv}}$ for the ogee wing yielded a value of about 7

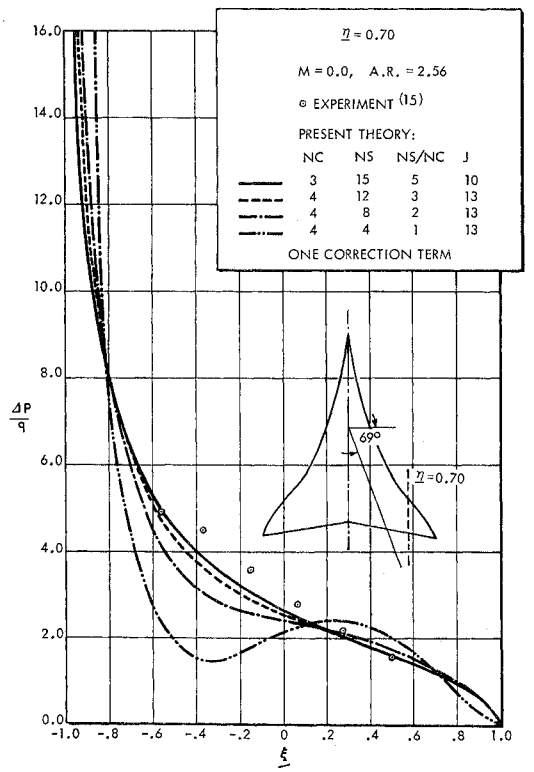

Fig. 7 Convergence of the predicted pressure distribution on an ogee wing.

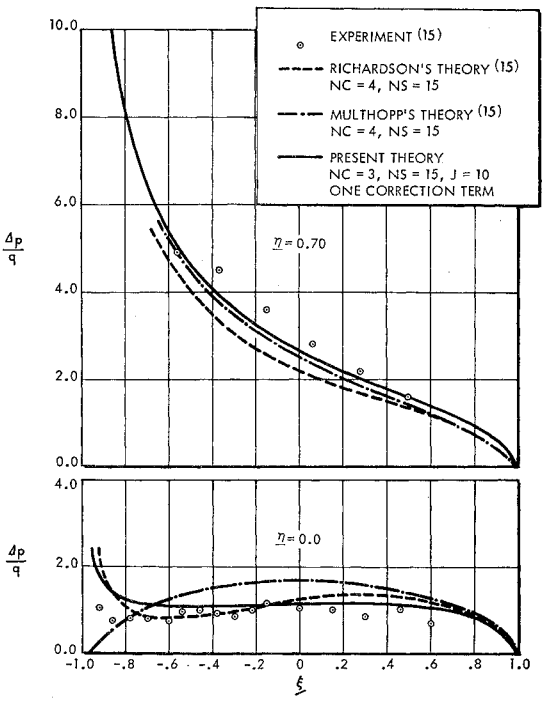

Fig. 8 Comparison of present theory with the theories of Multhopp and Richardson and with experiment on the ogee wing.

However, the results shown in Fig. 8 indicate that with $NS/NC = 5$, the present method agrees better with experiment than do the theories of Richardson and Multhopp.[15]

A final configuration was considered for which experimental data and other theoretical results were also available. Shown in Fig. 9 are the results from the present method and from both the experiment and Lamar's modified Multhopp theory.[4] With the values $NC = 3$, $NS = 15$, $J = 3$, and $P = 0$, very good agreement with experiment was obtained. The predicted value of $(NS/NC)_{\text{conv}}$ was 7.9 as obtained in Eq. (23). It is felt that a somewhat higher value for NS should have

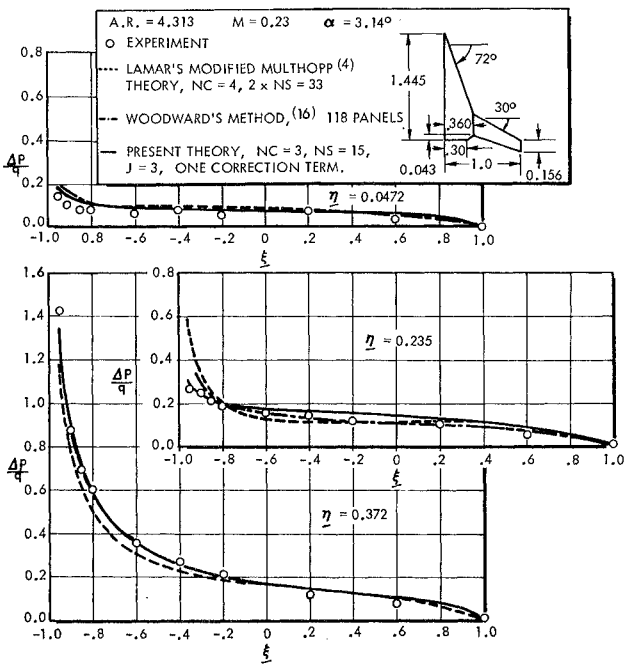

Fig. 9 Comparison of present theory with other theories and experiment on a variable sweep configuration.

been used; however, this was not possible with the computer program as it presently exists. Even with this restriction the results are very encouraging.

Shown also in Fig. 9 are the theoretical results as obtained by Bradley and Miller[16] with the Woodward finite-element method. For this case, the wing is represented with an array of 118 panels with a heavier concentration about the breakchord. The present method agrees very well with the Woodward method at both span stations $\mathbf{n} = 0.0472$ and $\mathbf{n} = 0.372$. At the station $\mathbf{n} = 0.235$, the Woodward procedure gives better agreement with experiment along the midchord, whereas the present theory is better near the leading edge. One should note that for the small differences in accuracy, the present method required only 45 downwash points as compared with 118 panels for the Woodward method. Hence, although the present method is not as flexible with regard to control surfaces, it is clearly more efficient than finite-element methods for predicting pressure distributions over isolated planar wings.

As a result of these applications, the values of NS/NC found to give converged (or nearly so) results were plotted against the parameter $\beta(AR)/\cos\Lambda_m$, as shown in Fig. 10. A mean line faired through the points indicates that nearly converged solutions can be obtained with the equation

$$(NS/NC)_{\text{conv}} = 0.8\ \beta(AR)/\cos|\Lambda_m| \qquad (24)$$

This is not rigorous since it is of an entirely empirical origin; however, it has been found to repeatedly yield very dependable solutions to lifting-surface problems. The values for NC in all cases presented in this paper have been 3 or greater. It has been found that no real significant changes occur when using NC values greater than 3. However, in data not presented here, $NC = 2$ does produce decidedly different results. Highly cambered surfaces may sometimes require more than a parabolic representation of the chordwise downwash variation; hence $NC > 3$ would certainly have to be used in these cases. (For further discussion of application to cambered surfaces, see Refs. 17 and 18 in this volume.)

Conclusions

It has been shown how inconsistent treatment of the chordwise discontinuity in Hsu's method for steady subsonic flow over planar surfaces will cause the solution to diverge with increasing downwash chords if the chordwise integral has not converged. This finding provides an explanation for the numerical results of Rowe, where such a trend was encountered.

As a result of this knowledge, a new equation for the quadrature integration of the product of the pressure and kernel functions is derived which contains correction terms accounting for the discontinuity and singularity of the steady-flow kernel function. This expression yields stable and accurate values for the integrals without resorting to a large number of integration points.

An optimum relationship determined between the chordwise downwash and integration points avoids the erratic variation of the chordwise integral with excess integration points as was shown by Rowe. This relationship preserves the interdigital nature of the downwash and integration points, which is necessary to achieve an integral value of minimum error.

The present method for predicting subsonic pressure distributions over planar surfaces is verified through comparison with experiment and other theories for a wide variety of planforms. As a result, an empirical relationship for this method is arrived at which specifies an optimum ratio of total spanwise to chordwise downwash points on the semispan that will produce a converged solution of acceptable accuracy. This ratio varies directly with β and aspect ratio and inversely with $(\cos|\Lambda_m|)$, where Λ_m is the average of the absolute leading and trailing edge sweeps.

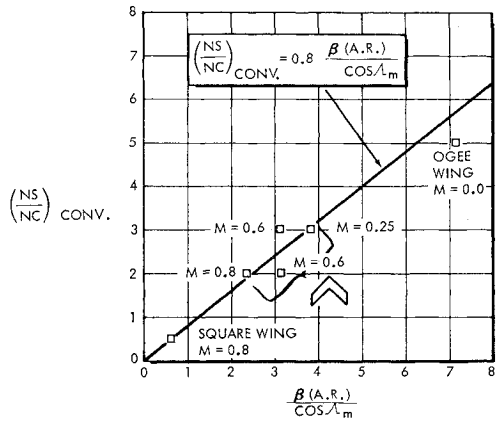

Fig. 10 NS/NC values for solutions shown which indicate convergence and their relationship with $\beta(AR)/\cos\Lambda_m$.

By comparison with two different finite-element methods, the present method is shown to be far more efficient for achieving an equivalent accuracy. Hence, because of the decreased number of chordwise integration points necessary for solution convergence, and the fact that it can solve planar surface problems with a minimum of control points, the present method provides a basis for developing an efficient and economical means for solving subsonic, oscillatory, lifting-surface problems. For further discussion of various aspects of this paper, refer to Refs. 17 and 18 in this volume.

References

[1] Albano, E. and Rodden, W. P., "A Doublet Lattice Method for Calculating Lift Distributions on Oscillating Surfaces in Subsonic Flow," *AIAA Journal*, Vol. 7, No. 2, Feb. 1969.

[2] Woodward, F. A., "A Unified Approach to the Analysis and Design of Wing-Body Combinations at Subsonic and Supersonic Speeds," AIAA Paper 68-55, New York, 1968.

[3] Multhopp, H., "Method for Calculating the Lift Distribution of Wings (Subsonic Lifting Surface Theory," Rept. AERO. 2353, Jan. 1950, Royal Aircraft Establishment, Farnborough, England.

[4] Lamar, J. E., "A Modified Multhopp Approach for Predicting Lifting Pressures and Camber Shape for Composite Planforms in Subsonic Flow," TN D-4427, July 1968, NASA.

[5] Hsu, P. T., "Flutter of Low Aspect-Ratio Wings, Part I, Calculation of Pressure Distributions for Oscillating Wings of Arbitrary Planform in Subsonic Flow by the Kernel-Function Method," TR 64-1, Oct. 1957, Massachusetts Institute of Technology, Cambridge, Mass.

[6] Rowe, W. S., "Collocation Method for Calculating the Aerodynamic Pressure Distributions on a Lifting Surface Oscillating in Subsonic Compressible Flow," *AIAA Symposium on Structural Dynamics and Aeroelasticity*, Boston, Mass., Aug. 30–Sept. 1, 1965, p. 31.

[7] Cunningham, A. M., Jr., "On the Treatment of the Kernel Function Singularities in the Integral Equation of Unsteady Subsonic Lifting Surface Theory," ERR-FW-746, 17 Aug. 1968, Fort Worth Division of General Dynamics, Fort Worth, Texas.

[8] Watkins, C. E., Woolston, D. S., and Cunningham, H. J., "A Systematic Kernel Function Procedure for Determining Aerodynamic Forces on Oscillating or Steady Finite Wings at Subsonic Speeds," TR-R-43, 1959, NASA.

[9] Stark, V. J. E., "The Tangent Plane Method and Polar Coordinates—A New Approach in Lifting Surface Theory," AIAA Paper 70-78, New York, 1970.

[10] Landahl, M. T. and Stark, V. J. E., "Numerical Lifting Surface Theory—Problems and Progress," *AIAA Journal*, Vol. 6, No. 11, Nov. 1968, pp. 2049.

[11] Kopal, Z., *Numerical Analysis*, Wiley, New York, 1955.

[12] Kulakowski, L. J. and Haskell, R. N., "Solution of Subsonic

Nonplanar Lifting Surface Problems by Means of High-Speed Digital Computers," *Journal of the Aerospace Sciences*, Vol. 28, Feb. 1961, p. 103–113.

[13] Lessing, H. C., Troutman, J. L., and Menees, G. P., "Experimental Determination of the Pressure Distribution on a Rectangular Wing Oscillating in the First Bending Mode for Mach Numbers from 0.24 to 1.30," TN D-344, Dec. 1960, NASA.

[14] Kolbe, C. D. and Boltz, F. W., "The Forces and Pressure Distribution at Subsonic Speeds on a Planar Wing Having 45° of Sweep Back, an Aspect Ratio of 3, and a Taper Ratio of 0.5," RM A51G31, Oct. 1951, NACA.

[15] Basu, B. C., "Aerodynamic Characteristics of Delta Type Wings with Curved Leading Edges at Subsonic Speeds," Rept. 26 396, F.M. 3529, Nov. 1964, Aeronautical Research Council.

[16] Bradley, R. G. and Miller, D. B., "Lifting Surface Theory—Advances and Applications," AIAA Paper 70-192, New York, 1970.

[17] Revell, J. D., "Comments on An Efficient Steady Subsonic Collocation Method for Solving Lifting Surface Problems," *Journal of Aircraft*, Vol. 8, No. 3, March, 1971, pp. 191.

[18] Cunningham, A. M., Jr., "Reply by Author to J. D. Revell," *Journal of Aircraft*, Vol. 8, No. 3, March 1971, pp. 192.

MARCH 1971 J. AIRCRAFT VOL. 8, NO. 3

Laminar, Transition, and Turbulent Boundary-Layer Characteristic with Favorable Pressure Gradient $M_1 = 9.6$

H. T. NAGAMATSU,* D. C. WISLER,† AND R. E. SHEER JR.‡
General Electric Research and Development Center, Schenectady, N. Y.

The effects of pressure gradient and roughness on the laminar boundary-layer transition and the characteristics of laminar, transition, and turbulent boundary layers were investigated in a hypersonic shock tunnel with a 4-ft long 10° cone. By maintaining a stagnation temperature of approximately 1400°K, the ratio of surface to stagnation temperature was 0.214, and the Mach number range over the heat gages was 7.8–10.2. Fast response platinum heat gages were used on the cone surface and the small wedge to detect the transition, the passage of turbulent bursts, and the local heat transfer rates. Boundary-layer surveys were conducted with impact pressure, total temperature, and wedge heat transfer probes to verify the existence of different types of boundary layers. From these measurements the characteristics of laminar, transition, and turbulent boundary layers were determined for a Mach number of 9.6. The experimental local heat transfer rates agreed reasonably well with the laminar theory and the turbulent theory which included both the density and velocity fluctuation terms.

Nomenclature

C_f = local skin-friction coefficient
C_h = local heat transfer coefficient
H_0 = freestream stagnation enthalpy
H_w = model wall enthalpy
l = Prandtl mixing length parameter
M = Mach number
P = pressure, psia
P'_o = freestream pitot pressure
P'_{o_4} = boundary-layer pitot pressure
q = local heat transfer rate, Btu/ft²-sec
Re_x = Reynolds number based on cone surface distance
Re_{δ^*} = Reynolds number based on displacement thickness
Re_θ = Reynolds number based on momentum thickness
T = temperature
u = local velocity
$\bar{u}$ = mean local velocity in turbulent boundary layer
x = distance along cone surface
y = distance normal to model wall
β = compressibility mixing length parameter
δ = local boundary-layer thickness
δ^* = displacement thickness
θ = momentum thickness
ρ = local density
$\bar{\rho}$ = mean local density in turbulent boundary layer
σ = Prandtl number
τ_w = local turbulent shear stress

Subscripts

0 = stagnation conditions
1 = local conditions outside boundary layer
5 = nozzle reservoir conditions

Received August 8, 1969; revision received April 8, 1971. This research was partially supported by the Ballistics Systems Division, United States Air Force.

* Research Associate. Associate Fellow AIAA.
† Aerospace Engineer; presently at the University of Colorado at Boulder, Colo. Associate Member AIAA.
‡ Fluid Mechanics Engineer. Member AIAA.

I. Introduction

THE knowledge regarding the laminar boundary-layer transition, local heat transfer rate, and skin friction for laminar and turbulent boundary layers at high Mach numbers is necessary for the design and development of advanced hypersonic vehicles, satellites, and space probes. Skin friction, ease of boundary-layer separation, and heat transfer rate depend upon whether the boundary layer is laminar or turbulent. There is a need for theoretical and experimental information on the effects of roughness, bluntness, pressure gradient, Mach number, real gas, wall cooling, and angle of attack on the transition Reynolds number at hypersonic Mach numbers. These effects have been investigated on 4- and 8-ft long 10° cones; some of the results are presented in Refs. 1–6.

At subsonic velocities, it was shown[7] that transition is a process involving the formation of turbulent spots, as postulated by Emmons.[8] This phenomenon is clearly visible in smoke tunnel photographs.[9] Turbulent bursts in the transition region were observed optically in the firing range[10,11] at supersonic speeds. Potter and Whitfield[12] investigated the